scientific reports

Check for updates

OPEN

SLC45A2 drives prostate cancer progression through tumor promotion and immune suppression

Run Tang, Cheng Wang, Yingxiang Zhu, Kai Liu & Zeming Wu✉

Prostate adenocarcinoma (PRAD) remains a leading cause of cancer-related mortality in men, highlighting an urgent need to identify novel prognostic biomarkers and therapeutic targets. While the role of solute carrier family genes in tumorigenesis has become increasingly well-defined, the function of the transmembrane transporter SLC45A2 in PRAD progression and immune regulation remains unclear. Transcriptomic data from 499 PRAD tumors and 52 normal tissues in the TCGA-PRAD database were integrated. Differentially expressed genes were screened using DESeq2, and independent prognostic genes were identified via Cox regression analysis (adjusted for age, TNM stage, and metastasis status). The expression of SLC45A2 in PRAD cell lines was verified by qRT-PCR and Western blot. CCK-8, wound-healing, and Transwell assays were performed to evaluate the effects of SLC45A2 on cell proliferation and migration. The infiltration levels of 24 immune cell types were analyzed using the ssGSEA algorithm. IHC and HPA database validated tissue-level protein expression. In vivo experiment was xenograft tumor model. The immunomodulatory role of SLC45A2 was explored via co-culture experiments of DU145 cells and $CD8^+$T cells. SLC45A2 was identified as an independent prognostic factor for PRAD. Its mRNA and protein levels were significantly upregulated in tumor tissues compared to normal tissues. Functional experiments showed that SLC45A2 knockdown inhibited the proliferation and migration of LNCaP and DU145 cells, while SLC45A2 overexpression reversed these effects. Mechanistically, SLC45A2 promoted PRAD cell proliferation by activating the PI3K/AKT pathway and mediated immune evasion by impairing the cytotoxic effect of $CD8^+$T cells. SLC45A2 drives PRAD progression via dual oncogenic mechanisms: direct promotion of tumor proliferation and migration, and suppression of cytotoxic immune cell infiltration, confirming that SLC45A2 can serve as a potential prognostic biomarker and therapeutic target for advanced PRAD.

Keywords Prostate adenocarcinoma, SLC45A2, Immune evasion, Prognostic biomarker, Tumor metabolism

Prostate adenocarcinoma (PRAD) is the second most diagnosed malignancy in men globally, with over 1.4 million new cases reported in 2020. Despite the significant improvements in early diagnostic efficiency brought about by prostate-specific antigen screening and the Gleason scoring system, patients with metastatic PRAD still face a 5-year survival rate of less than 30% due to chemotherapy resistance and limited targeted therapeutic options[1–3]. The genomic heterogeneity of PRAD revealed by the Cancer Genome Atlas (TCGA) database indicates that a single biomarker or therapeutic target is insufficient to meet clinical needs, highlighting an urgent requirement to identify key molecules driving tumor progression from multiple dimensions, such as metabolism and immunity[4,5].

As the second largest membrane protein family in humans, the solute carrier (SLC) family participates in tumor metabolic reprogramming by regulating nutrient uptake, ion transport, and drug transport processes hijacked in cancer[6,7]. Accumulating evidence has confirmed that members of the SLC family exert oncogenic effects in various cancers. High expression of SLC2A1 is associated with poor prognosis in lung adenocarcinoma[7], and SLC39A5 promotes the proliferation of lung adenocarcinoma cells by activating the PI3K/AKT pathway[8]. More importantly, some SLC proteins can mediate immune evasion by remodeling the tumor microenvironment; examples include SLC16A3, which induces T-cell exhaustion through lactate efflux, and SLC7A5, which inhibits T-cell function via tryptophan depletion[9]. However, the function of the transmembrane transporter SLC45A2,

Department of Urology, The People's Hospital of Suzhou New District, NO.95 Huashan Road, Suzhou 215000, China. ✉email: 18006209937@163.com

which is also a member of the SLC family, in PRAD remains largely unexplored. Previous studies have only reported that SLC45A2 affects metastasis in melanoma by regulating melanosomal glycolysis[9,10], while its roles in metabolic regulation and TME shaping in PRAD have not been documented.

PRAD is characterized by a typical "cold tumor" phenotype, manifested as insufficient $CD8^+$T cell infiltration and enrichment of regulatory T cells and myeloid-derived suppressor cells. This feature greatly limits the efficacy of immune checkpoint inhibitors[11]. Emerging evidence implicates SLC transporters in shaping immunometabolic landscapes: SLC7A5-mediated tryptophan depletion impairs T-cell function[12], while SLC16A3 drives lactate-mediated immuno-suppression[3,13]. However, whether SLC45A2 modulates PRAD's immune microenvironment remains unknown. Recent studies have suggested a close crosstalk between metabolism-related genes and immune cell function. Alpha-methylacyl-CoA racemase (AMACR), a well-established diagnostic biomarker for prostate adenocarcinoma (PRAD), is known to mediate abnormal fatty acid metabolism, which may compromise anti-tumor immunity by altering the energy supply of immune cells[14,15]. Moreover, previous studies have reported a potential link between AMACR and the PI3K/AKT signaling pathway[16]. Notably, our preliminary co-expression network analysis identified a strong co-expression pattern among SLC45A2, AMACR, and albumin (ALB), suggesting that these genes may cooperatively regulate metabolic processes and thereby influence PRAD progression. However, this hypothesis remains to be experimentally validated.

Based on the aforementioned research gaps, we hypothesized that SLC45A2 drives prostate adenocarcinoma (PRAD) progression through a dual mechanism of metabolic regulation and immune evasion. Specifically, we aim to determine whether SLC45A2 drives tumor proliferation and migration through activation of the AMACR, PI3K/AKT pathway, while concurrently inhibiting the infiltration of cytotoxic immune cells, including $CD8^+$ T cells. To test this hypothesis, we integrated multi-omics analyses from the TCGA-PRAD dataset with in vitro functional assays (including proliferation, migration, apoptosis, and co-culture experiments) to comprehensively elucidate the role and mechanism of SLC45A2 in PRAD. Ultimately, this study aims to identify SLC45A2 as a potential molecular target for prognostic evaluation and precision therapy in prostate cancer.

Materials and methods

Data acquisition and preprocessing

Data Retrieval and Pretreatment: Transcriptome data (RNA-seq in FPKM/TPM format) and corresponding clinical information for prostate adenocarcinoma (PRAD) were downloaded from The Cancer Genome Atlas (TCGA) database (https://portal.gdc.cancer.gov/). Tumor samples were selected based on the annotation "Primary Tumor" (TCGA sample codes ending in "01") for transcriptome profiling. Normal controls were non-cancerous tissue data labeled as "Solid Tissue Normal" (codes ending in "11"). Cases with complete overall survival (OS) time and survival status (Alive/Dead) were extracted from the clinical dataset.

Differential expression analysis

Raw expression matrices were normalized using the "DESeq2 R" package[17], and low-expression genes were filtered out (threshold: >50% of samples with FPKM/TPM > 1). Differential expression analysis between tumor and normal tissues was conducted using a negative binomial generalized linear model. Genes with $|\log2FoldChange| \geq 1$ and false discovery rate-adjusted p-values < 0.05 were considered significant.

Identification of independent prognostic genes

Transcriptome data were merged with prognostic information, excluding cases with survival times ≤ 30 days or duplicate samples. Univariate Cox proportional hazards models were performed using the "survival R" package[18], with gene expression as the predictor and OS as the outcome. Genes with $P < 0.05$ were selected as candidate prognostic genes. These were further validated for independent prognostic value ($P < 0.05$) in the presence of clinical covariates such as age and TNM stage. Differentially expressed genes (DEGs) were intersected with prognostic genes to identify candidates involved in both tumorigenesis and survival regulation. Kaplan-Meier analysis (log-rank test, $P < 0.05$) was conducted to assess the prognostic stratification ability of intersected genes using the survminer R package (v0.4.9). The correlation between high/low SLC45A2 expression and clinicopathological factors was also evaluated.

Immune infiltration analysis

RNA-seq data from the TCGA-PRAD project, processed through the STAR pipeline, were downloaded and organized in TPM format, along with clinical data, excluding normal samples. Immune infiltration was calculated using the ssGSEA algorithm from the "GSVA R" package[19]based on 24 immune cell markers provided in the Immunity article. The correlation between SLC45A2 and immune infiltration was analyzed, and results were visualized using lollipop plots.

HPA database analysis of SLC45A2 expression

The Human Protein Atlas (HPA) is an open resource providing detailed information on human protein expression patterns. HPA database analysis was conducted to investigate SLC45A2 expression across different tissues, cell types, and disease states. Specifically, we analyzed the differential expression of SLC45A2 in prostate cancer versus adjacent non-cancerous tissues. Semi-quantitative scoring (0, no expression; 1+, weak; 2+, moderate; 3+, strong) based on immunohistochemical staining intensity was performed. Statistical measures, including mean and standard deviation, were calculated to assess differences between the two groups.

Cell culture and plasmid construction

Cells used in this study were purchased from the Chinese Academy of Medical Sciences. LNCap and DU145 cells were cultured in DMEM medium supplemented with 10% fetal bovine serum until reaching the logarithmic

growth phase. On the day before transfection, cells were plated at appropriate densities. SLC45A2 knockdown and overexpression plasmids were extracted from Escherichia coli using a plasmid extraction kit. Plasmid concentration and purity were determined using a spectrophotometer. Based on cell density and transfection reagent instructions, appropriate amounts of plasmid and transfection reagent were mixed, incubated at room temperature to form transfection complexes, and gently added to the cell culture medium. Cells were then incubated under appropriate conditions (typically 24–48 h) to allow plasmid entry and expression. Transfection efficiency was verified by RT-qPCR or Western blot for knockdown and overexpression confirmation. Further functional studies, such as cell proliferation, migration, and apoptosis assays, were performed on transfected cells.

Quantitative real-time polymerase chain reaction (qRT-PCR)

Sample Preparation and RNA Extraction Optimization: cDNA samples were thawed on ice, and an 8-well PCR tube reaction system was prepared with three replicates per sample for data reliability. After mixing in the dark, samples were centrifuged to remove bubbles and placed in a PCR machine for amplification and detection. RNA extraction was optimized by selecting cells at the logarithmic growth phase with 70%-80% confluence. Cells were washed with PBS and lysed with TRleasy reagent in RNase-free EP tubes. Chloroform was added, vortexed, and allowed to sit for phase separation. The upper aqueous phase was collected after centrifugation, and RNA was precipitated with isopropanol, washed with 80% ethanol, air-dried, and dissolved in DEPC water. RNA concentration was measured, and samples were stored at -80 °C.

Reverse Transcription: RNA samples were thawed on ice and prepared for gDNA digestion based on concentration. After digestion, reverse transcription components were added to construct the reaction system, mixed, centrifuged, and incubated in a PCR machine. The resulting cDNA was diluted with water and stored at -20 °C.

qPCR Detection: cDNA samples were thawed on ice, and a PCR tube reaction system with three replicates was prepared. After mixing in the dark and centrifuging, samples were placed in a PCR machine for amplification and detection. Experimental conditions were strictly controlled for sterility to prevent RNA degradation and reagent denaturation, ensuring accurate and reliable results. Optimized RNA extraction and reverse transcription steps improved cDNA quality and quantity, providing a reliable template for subsequent qRT-PCR experiments. Primer sequences are in Table 1.

Western blot (WB) validation of SLC45A2 expression in normal prostate cells and PRAD cells

Normal prostate epithelial cells and multiple PRAD cell lines were cultured and stored in liquid nitrogen to maintain biological activity. Total protein was extracted using ice-cold RIPA lysis buffer containing protease and phosphatase inhibitors, followed by SDS-PAGE electrophoresis for protein separation. Proteins were transferred to PVDF or nitrocellulose membranes, blocked with TBST containing skim milk, and incubated overnight at 4 °C with a specific antibody against SLC45A2 (purchased from Abcolonal, cat. no. PA5-99036). Membranes were then incubated with HRP-labeled secondary antibody, treated with chemiluminescent substrate solution, and visualized using a chemiluminescent imaging system. Quantitative analysis of Western blot bands was performed using image analysis software to assess SLC45A2 expression differences between normal prostate cells and PRAD cells, providing crucial data for further biological research and clinical applications.

CCK-8 assay to evaluate the effect of SLC45A2 expression on PRAD cell proliferation

Normal and PRAD cell lines were thawed, rapidly recovered, and cultured in a medium containing appropriate growth factors. Cells were maintained in a 37℃, 5% CO2 incubator until reaching the logarithmic growth phase. Cells were trypsinized to prepare single-cell suspensions and cell concentrations were adjusted to ensure consistent cell numbers per well. Cell suspensions (100 µl per well, containing approximately 2,000 cells for proliferation experiments) were plated in 96-well plates. Experimental groups included SLC45A2 knockdown, overexpression, and empty vector controls. CCK-8 solution (10 µl) was added to each well at specified time points (e.g., 0, 6, 24, 48, 72 h), and plates were incubated for 1–4 h based on cell type and density. Absorbance (OD values) were measured at 450 nm using a microplate reader. Cell viability or proliferation rates were calculated using the formula: Cell viability/proliferation rate = [(As - Ab) / (Ac - Ab)] × 100%, where As is the OD value of the experimental well, Ac is the OD value of the control well, and Ab is the OD value of the blank well. Statistical analysis (t-test or ANOVA) was performed using software (e.g., SPSS, GraphPad Prism) to determine significant differences between groups. Cell growth curves were plotted to visually demonstrate the impact of SLC45A2 knockdown and overexpression on PRAD cell proliferation.

Gene	Primer sequences 5′–3′
SLC45A2	Forward Primer: CTGGCCGCCACATCTATAAAT Reverse Primer: GTAGCAGAACTCTCTTCCGAAC
Actin	Forward Primer: GGAGCGAGATCCCTCCAAAAT Reverse Primer: GGCTGTTGTCATACTTCTCATGG

Table 1. Primer sequences.

Wound healing assay to verify the effect of SLC45A2 expression on the migration ability of PRAD cells

PRAD cell lines were cultured in RPMI-1640 medium supplemented with 10% fetal bovine serum and maintained in a humidified incubator at 37 °C with 5% CO2 until they reached the logarithmic growth phase. Using Lipo3000 transfection reagent, SLC45A2 knockdown plasmids and overexpression plasmids were introduced into PRAD cells, respectively, with an empty plasmid control group set up simultaneously. After transfection, the cells were further cultured for an appropriate period to ensure plasmid expression and cellular adaptation. Once the cells reached a suitable density, a uniform scratch was created on the monolayer of cells using a sterile pipette tip or a cell scratch tester. The initial state of the scratch was recorded using a microscope, and the width and length of the scratch were measured to calculate the initial scratch area. The cells were then continued to be cultured in a medium containing an appropriate concentration of serum to observe scratch healing. At predetermined time points (e.g., 6 h, 12 h, 24 h, etc.), the healing of the scratch was recorded using a microscope, and the width and length of the scratch were measured to calculate the scratch area at time t. Based on the initial scratch area and the scratch area at time t, the cell migration rate was calculated as follows: Cell Migration Rate = (Initial Scratch Area - Scratch Area at Time t) / Initial Scratch Area × 100%. Statistical software was used to perform t-tests or ANOVA on the experimental data to determine whether there were significant differences between different experimental groups. A curve graph of cell migration rate over time was plotted to visually demonstrate the effect of SLC45A2 knockdown and overexpression on the migration ability of PRAD cells.

Immunohistochemistry (IHC)

Slides were deparaffinized and subjected to heat-induced antigen retrieval in citrate buffer (pH 6.0). Immunohistochemistry was performed using a streptavidin-biotin-peroxidase method with diaminobenzidine (DAB) as the chromogen (Kit LSAB, Dakocytomation, Glostrup, Denmark). The primary antibody used was against SLC45A2. Negative controls were included by either omitting the primary antibody or using an irrelevant antibody.

SLC45A2 staining was independently evaluated by two blinded observers, including a pathologist, and consensus scores were determined for each tissue core. Staining intensity was graded on a scale of 0 to 3 (0 = no staining, 1 = weak, 2 = moderate, 3 = strong), and the percentage of SLC45A2-positive cells was scored as follows: 0 (0%), 1 (1–33%), 2 (34–66%), and 3 (67–100%). In cases of discrepancy between duplicate cores, the higher score was used as the final value. The final staining score was calculated by summing the intensity and percentage scores and was categorized as follows: 0, negative; 1–2, weak; 3–4, moderate; and 5–6, strong[20].

Cell apoptosis analysis

All cells were seeded in 6-well plates (5×10^5 cells/well) and transfected with si-SLC45A2 for 24–72 h. After treatment, both adherent and floating cells were collected, washed twice with cold PBS, and resuspended in 1× binding buffer. Cells were stained with Annexin V-FITC and propidium iodide (PI) for 15 min at room temperature in the dark, followed by flow cytometry analysis (excitation 488 nm). Apoptotic cell percentages were quantified using FlowJo software.

In vivo tumor growth assay

Male nude mice were subcutaneously injected with either control or SLC45A2-overexpressing prostate cancer cells. For the tumor growth assay, 1×10^6 cells were inoculated subcutaneously into six-week-old male athymic mice. Tumor dimensions were measured every three days, and volumes were calculated using the formula: (length × width^2) / 2. All mice were anesthetized with sodium pentobarbital (50 mg/kg, intraperitoneally) prior to euthanasia. Euthanasia was then performed by CO_2 inhalation (35% vol/min) in a chamber ($630 \times 480 \times 500$ mm), in accordance with the AVMA Guidelines for the Euthanasia of Animals (2020) and approved institutional protocols. CO_2 exposure was maintained for at least one minute after respiration had ceased. Death was confirmed by the absence of heartbeat and respiration, development of rigor mortis, and dilated pupils. All animal experiments were conducted in compliance with institutional guidelines and approved by the Ethical Committee of the People's Hospital of Suzhou New District. The study adhered to the principles of the Declaration of Helsinki and was reported in accordance with the ARRIVE guidelines.

Transwell assay

Transwell inserts were placed in 24-well plates containing 700 µL of medium with 10% FBS. All cells were resuspended in serum-free medium (2×10^5 cells/mL), and 150 µL of suspension was added to each upper chamber. After 24 h of incubation, cells were fixed with 4% paraformaldehyde and stained with crystal violet for 30 min. Non-migrated cells were removed, and migrated cells on the lower membrane were counted under a microscope in randomly selected fields.

Co-culture assay

DU145 cells (5×10^3/mL) were seeded in 96-well plates and co-cultured with activated CD8$^+$ T cells (5×10^4/mL, ratio 1:10). Three groups were included: control, DU145 monoculture, and DU145–CD8$^+$ T co-culture. After 7–10 days of incubation, colonies were fixed with 4% paraformaldehyde, stained with 0.1% crystal violet, and counted under a microscope. Colonies > 50 µm were quantified, and averages from replicate wells were used for statistical analysis.

Functional annotation and pathway enrichment analysis

Gene Ontology (GO) and Kyoto Encyclopedia of Genes and Genomes (KEGG) pathway enrichment analyses[21–25] were performed using the Database for Annotation, Visualization, and Integrated Discovery (DAVID) platform (https://david.ncifcrf.gov/.

) with a significance threshold of $P < 0.05$.

Statistical analysis

In this study, we conducted an in-depth analysis of microarray data using R language, including linear modeling of the data and identification of differential expression. To compare expression differences between different sample groups, we performed Wilcoxon rank-sum tests as well as t-tests and set $P < 0.05$ as the threshold for statistical significance. The software used in our study are listed as follows: SPSS Statistics, Version 26.0 (IBM Corp., Armonk, NY, USA); https://www.ibm.com/products/spss-statistics. GraphPad Prism, Version 9.0 (GraphPad Software, San Diego, CA, USA); https://www.graphpad.com. ImageJ, Version 1.53 (National Institutes of Health, USA); https://imagej.nih.gov/ij/. FlowJo, Version 10.8 (BD Biosciences, Ashland, OR, USA); https://www.flowjo.com.

Approval statement

All experimental protocols were approved by the medical ethical committee of The People's Hospital of Suzhou New District and has followed the principles outlined in the Declaration of Helsinki for all human or animal experimental investigations. Our study was reported as described by the ARRIVE guidelines.

Results

Identification of SLC45A2 as an independent prognostic factor for PRAD based on the TCGA database

Using the TCGA database, we identified differentially expressed molecules in TCGA-PRAD with an absolute value of LogFC greater than 2, resulting in a total of 965 differentially expressed genes (Figs. 1A–D). Additionally, we identified molecules associated with the prognosis of PRAD, yielding a total of 208 such molecules. By taking the intersection of these two gene sets, we obtained two overlapping molecules: SLC45A2 and AMPK2 (Fig. 1E). Subsequently, we conducted differential expression analysis at the mRNA level for these two molecules, which indicated that SLC45A2 was significantly overexpressed in tumor tissues compared to normal tissues (Fig. 1F). This was further confirmed by tissue-paired analysis (Fig. 1G) and the data from GSE35988 (Fig. 1H). To validate the relationship between SLC45A2 and the prognosis of PRAD patients, we found that patients with high SLC45A2 expression had a poorer prognosis compared to those with low SLC45A2 expression (Fig. 1I, $P = 0.041$).

Strong correlation between SLC45A2 expression and clinicopathological factors in PRAD

Based on the expression level of SLC45A2 in tissues, a median value was set, with values above it labeled as the high expression group and values below it as the low expression group. Through analysis of the PRAD population in the database, we found that patient prognosis was closely related to (Fig. 2A–B) age, (Fig. 2C–D) lymph node metastasis, (Fig. 2E–F) gender, (Fig. 2G–H) clinical stage, and (Fig. 2I–J) the presence or absence of distant metastasis. In other words, compared to the low-expression group of SLC45A2, patients in the high-expression group had a poorer prognosis. In addition, Table 2 confirms that pathological T and N staging, clinical T and M staging, and overall patient survival all show poor prognosis in the high expression group.

SLC45A2 enhances immunosuppressive cell expression in the PRAD tumor microenvironment

RNAseq data processed with the STAR pipeline and clinical data from the TCGA-PRAD project were downloaded, curated, and normalized to TPM (Transcripts Per Million) format, with normal tissue samples excluded. Immune infiltration profiles were computed using the ssGSEA algorithm based on 24 immune cell markers provided in the immunity study. Results revealed a significant negative correlation between SLC45A2 expression and the infiltration of cytotoxic immune cells (NK cells, CD8 + T cells), suggesting that elevated SLC45A2 expression in PRAD fosters an immunosuppressive microenvironment and promotes tumor progression (Fig. 3). Further mechanistic investigations are warranted to elucidate the underlying regulatory pathways.

SLC45A2 is significantly overexpressed in multiple prostate cancer cell lines

To validate the differential expression of SLC45A2 between normal prostate tissues and prostate cancer tissues, we first conducted qRT-PCR experiments in a normal prostate epithelial cell line (RWPE1) and multiple prostate cancer cell lines (LNCaP, PC3, DU145, 22Rv1, C4-2, NCI-H660, VCaP). Results revealed that SLC45A2 mRNA levels were significantly higher in prostate cancer cell lines compared to normal cells (Fig. 4A). Subsequent Western blot analysis confirmed consistent overexpression of SLC45A2 protein in cancer cells (Fig. 4B).

SLC45A2 overexpression is closely associated with PRAD cell proliferation and migration

Based on preliminary evidence from public databases and cellular experiments identifying SLC45A2 as an oncogenic factor in PRAD, we proceeded to perform knockdown and overexpression interventions in LNCaP cells to enable subsequent phenotypic and mechanistic studies. First, siRNA targeting SLC45A2 and overexpression plasmids were transfected into LNCaP cells. Results demonstrated that SLC45A2 mRNA and protein levels were significantly downregulated (Fig. 5A) and upregulated (Fig. 5B), respectively. Subsequent validation at the protein level confirmed consistency with qPCR findings (Fig. 5C). Collectively, these data confirm the effective modulation of SLC45A2 expression at both transcriptional and translational levels.

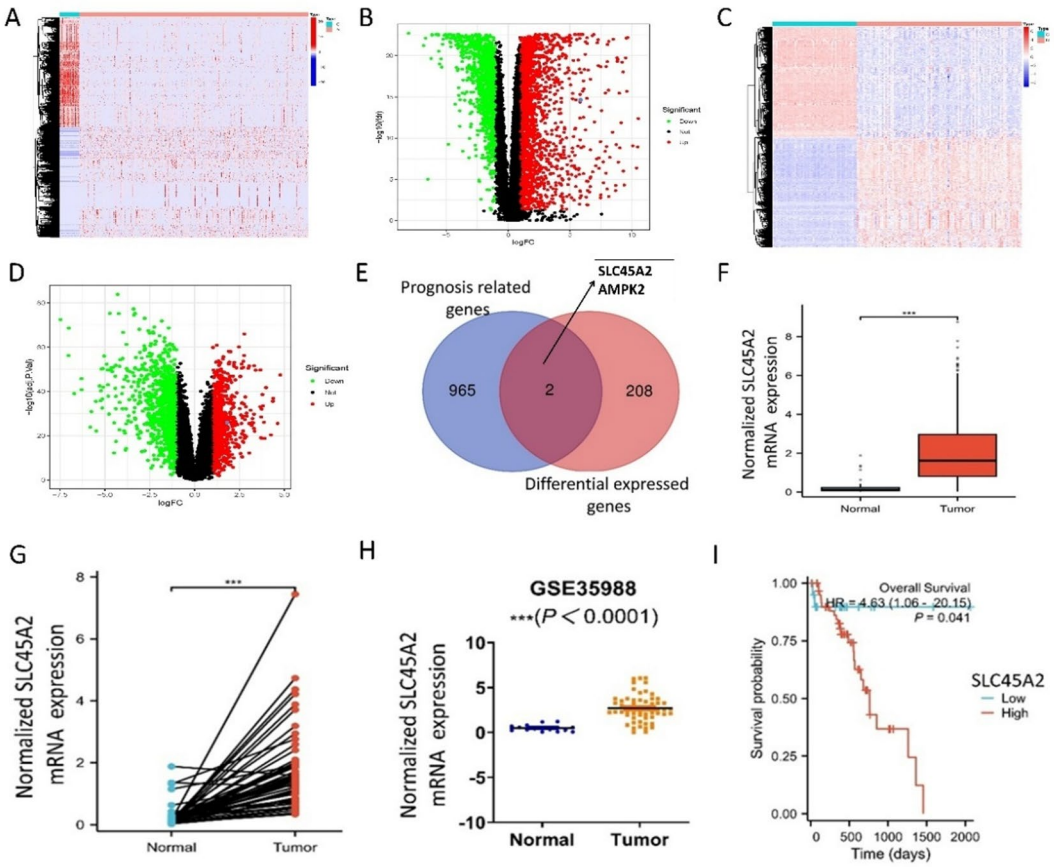

Fig. 1. SLC45A2 as an Independent Prognostic Factor for PRAD. (**A**–**B**) Heatmap and volcano plot of differentially expressed genes based on TCGA database analysis. Blue point: SLC45A2. (**C**–**D**) Heatmap and volcano plot of differentially expressed genes based on GSE35988 dataset analysis. Blue point: SLC45A2. (**E**) Combined analysis based on differentially expressed molecules and prognosis-related molecules in PRAD to identify independent prognostic-related molecules for PRAD. (**F**–**G**) Differential expression of SLC45A2 between normal tissues and tumor tissues based on the TCGA database. (**H**) SLC45A2 mRNA level was upregulated in prostate cancer in dataset GSE35988. (**I**) Overall survival analysis in PRAD based on high and low expression of SLC45A2.

To investigate the functional impact of SLC45A2 on PRAD cell proliferation and migration, we first performed CCK-8 assays. Results revealed that SLC45A2 knockdown significantly inhibited PRAD cell proliferation, while overexpression markedly enhanced it (Figs. 5D-E). To exclude the influence of apoptosis, we further validate the role of SLC45A2 in regulating PRAD cell apoptosis using flow cytometric analysis. In DU145 and LNCaP cells subjected to SLC45A2 knockdown, respectively, the results demonstrated that SLC45A2 silencing did not influence the apoptotic rate of PRAD cells (Fig. 5F). To evaluate the in vivo effects, a xenograft tumor model was established using DU145 cells. The subcutaneous xenograft assay demonstrated that SLC45A2 overexpression resulted in a significant increase in tumor volume over time and a greater final tumor weight compared with the control group (Fig. 5G).These results indicated that SLC45A2 overexpression resulted in promotion in cell proliferation.

To assess the role of SLC45A2 in prostate cancer cell migration, we performed knockdown and overexpression experiments in DU145 and LNCaP cells, respectively, and evaluated cell motility using Transwell assays. In the SLC45A2 knockdown group (Fig. 6A), the number of migrated cells was markedly decreased compared with the negative control. Conversely, in the SLC45A2 overexpression group (Fig. 6B), the number of migrated cells was significantly increased relative to the control group. Furthermore, wound-healing assays confirmed that SLC45A2 depletion significantly impaired PRAD cell migratory capacity (Figs. 6C-D). These results indicate that SLC45A2 can promote the migration of PRAD cells. Collectively, these findings demonstrate that SLC45A2 promotes malignant phenotypes in PRAD, suggesting that targeting SLC45A2 expression may represent a valuable therapeutic strategy for PRAD intervention.

Tissue expression analysis reveals differential SLC45A2 expression between PRAD tumors and adjacent normal tissues

By analyzing SLC45A2 expression patterns in tumor vs. adjacent non-tumor tissues from PRAD patients using the HPA database, we acquired data from three independent cases and performed clear visualization

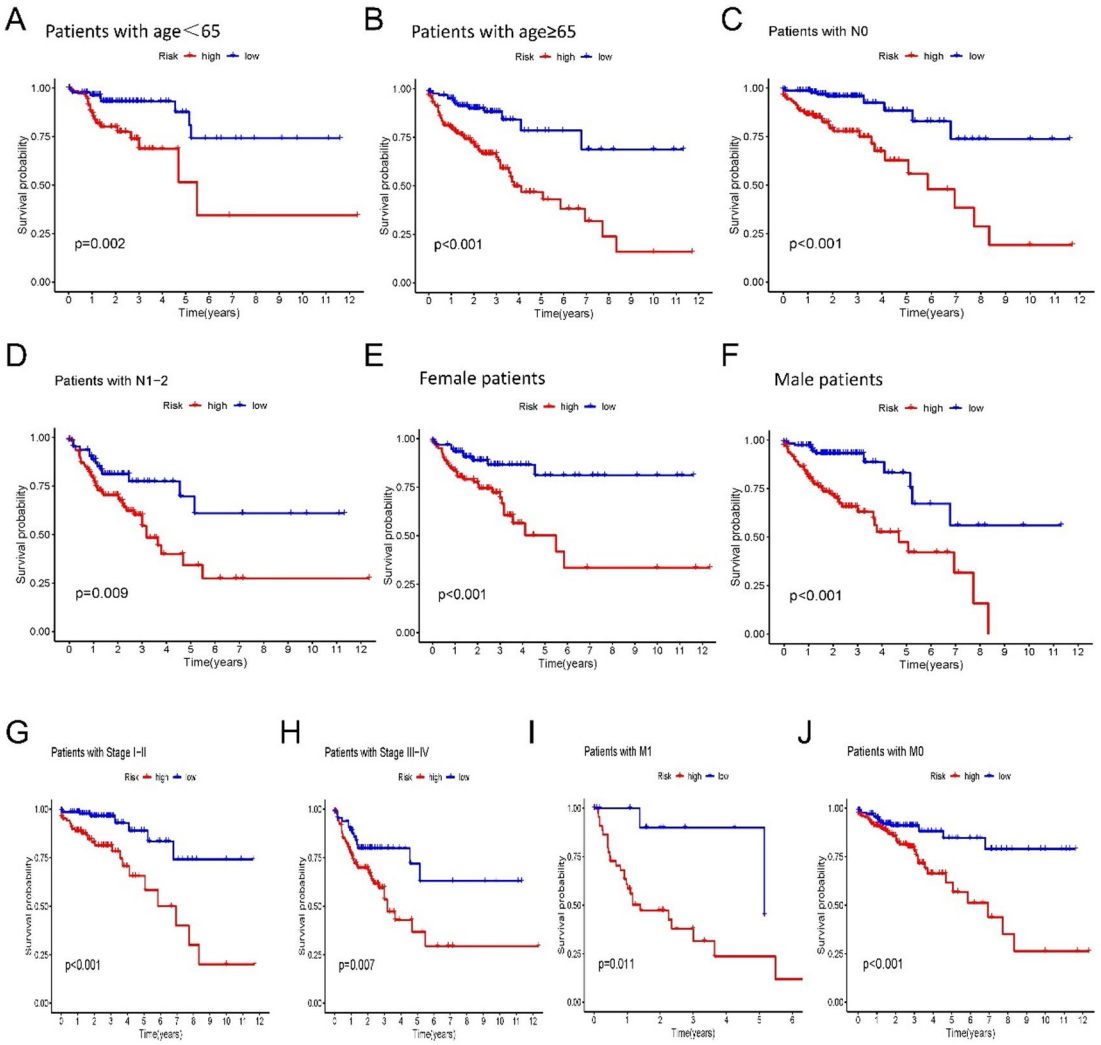

Fig. 2. Correlation analysis of SLC45A2 with clinicopathological factors in PRAD. Prognostic analysis of patients stratified by high vs. low SLC45A2 expression concerning (**A**–**B**) age, (**C**–**D**) lymph node metastasis, (**E**–**F**) gender, (**G**–**H**) clinical stage, and (**I**–**J**) presence of distant metastasis.

of SLC45A2 staining intensity across varying magnification levels. The results indicated that SLC45A2 was significantly overexpressed in PRAD tumor tissues compared to matched adjacent normal tissues (Fig. 6E). We also examined SLC45A2 expression by IHC in prostate cancer tissues and matched adjacent normal tissues. As shown in Fig. 6F, prostate cancer tissues showed much higher SLC45A2 expression in compared with benign prostatic epithelia.

Mechanism exploration and correlation analysis between SLC45A2 and AMACR/ALB

To further investigate the mechanisms by which SLC45A2 promotes prostate cancer progression, we retrieved the top 500 genes correlated with its expression from the prostate cancer dataset in the GEPIA2 database. GO (Fig. 7A) and KEGG (Fig. 7B) analyses revealed that SLC45A2-associated genes were mainly enriched in pathways related to cell proliferation, cell cycle regulation, and metabolism, which is consistent with our previous findings. During our investigation of SLC45A2's biological functions and differential expression patterns, we further confirmed the correlation between SLC45A2 and the molecules AMACR and ALB. Initially, we performed correlation analysis at the mRNA level using the TCGA database and observed a positive correlation among the three genes respectively (Figs. 7C and D). Subsequently, we validated this correlation at the protein expression level of patient tissues and found consistent results with the mRNA data (Fig. 7E). Moreover, SLC45A2 could promote AMACR expression in PRAD cells (Fig. 8A). Based on these findings, we hypothesize that SLC45A2 may interact with these two molecules through specific expression regulatory mechanisms.

SLC45A2 promotes PRAD cell proliferation and migration via the PI3K/AKT signaling pathway

Previous studies have reported a potential link between AMACR and the PI3K/AKT signaling pathway[16]. To investigate how SLC45A2 could promote AMACR expression in PRAD cells, we then explored the impact of

Characteristics	Low expression of SLC45A2	High expression of SLC45A2	*P* value
n	157	140	
Age, n (%)			0.176
< = 60	64 (21.5%)	68 (22.9%)	
> 60	93 (31.3%)	72 (24.2%)	
Pathologic T stage, n (%)			0.040
T2	98 (33%)	4 (1.3%)	
T3	55 (18.5%)	85 (28.6%)	
T4	4 (1.3%)	51 (17.2%)	
Pathologic N stage, n (%)			0.048
N0	129 (43.4%)	27 (9.1%)	
N1	28 (9.4%)	113 (38%)	
Clinical T stage, n (%)			0.024
T1	71 (23.9%)	20 (6.7%)	
T2	65 (21.9%)	1 (0.3%)	
T3	21 (7.1%)	45 (15.2%)	
T4	0 (0%)	74 (24.9%)	
Clinical M stage, n (%)			0.029
M0	155 (52.2%)	0 (0%)	
M1	2 (0.7%)	140 (47.1%)	
Primary therapy outcome, n (%)			0.018
PD	14 (4.7%)	113 (38%)	
SD	11 (3.7%)	12 (4%)	
PR	17 (5.7%)	5 (1.7%)	
CR	115 (38.7%)	10 (3.4%)	
OS event, n (%)			0.006
Alive	153 (51.5%)	2 (0.7%)	
Dead	4 (1.3%)	138 (46.5%)	
DSS event, n (%)			0.697
No	154 (51.9%)	139 (46.8%)	
Yes	3 (1%)	1 (0.3%)	
PFI event, n (%)			0.423
No	126 (42.4%)	107 (36%)	
Yes	31 (10.4%)	33 (11.1%)	

Table 2. TCGA database PRAD patient baseline data table.

SLC45A2 on the PI3K/AKT signaling pathway and the expression of related proteins. We employed Western blot analysis to detect the protein expression levels of p-PI3K, PI3K, p-AKT, AKT, AMACR, and PCNA (proliferation-related marker) in DU145 (Fig. 8A), with GAPDH serving as the internal reference. The results revealed that in si-SLC45A2-treated DU145 cells, the protein expression levels of p-PI3K, p-AKT, and PCNA were significantly lower than those in the control group. Conversely, in OE-SLC45A2-treated cells, the expression levels of these proteins were notably higher compared to the control group. There were no significant differences in the total protein expression of PI3K and AKT among the various groups.

To further verify the mediating role of the PI3K/AKT signaling pathway in SLC45A2-induced upregulation of AMACR expression, we treated SLC45A2 knockdown DU145 cells with the PI3K activator IGF-1 (10 nM) and found that IGF-1 partially restored AMACR expression (Fig. 8B). Furthermore, cell proliferation and migration assays showed that IGF-1 treatment rescued the inhibitory effects of SLC45A2 knockdown on cell proliferation and migration (Figs. 8C and D), providing additional evidence that SLC45A2 promotes prostate cancer cell proliferation and migration through the PI3K/AKT signaling pathway.

SLC45A2 regulates PRAD cell proliferation by modulating CD8⁺T cell

To investigate the impact of SLC45A2 knockdown on the killing effect of $CD8^+$T cells on DU145 cells, we conducted co-culture experiments. The results demonstrated that when only si-SLC45A2 was applied, the number of DU145 cells decreased compared to the control group (where SLC45A2 was not knocked down and no $CD8^+$T cells were present). When only $CD8^+$T cells were added, there was also a certain degree of reduction in the cell number. Notably, when SLC45A2 was knocked down simultaneously with the addition of $CD8^+$T cells, the number of DU145 cells decreased significantly. This indicates that SLC45A2 knockdown can enhance the killing effect of $CD8^+$T cells on DU145 cells.

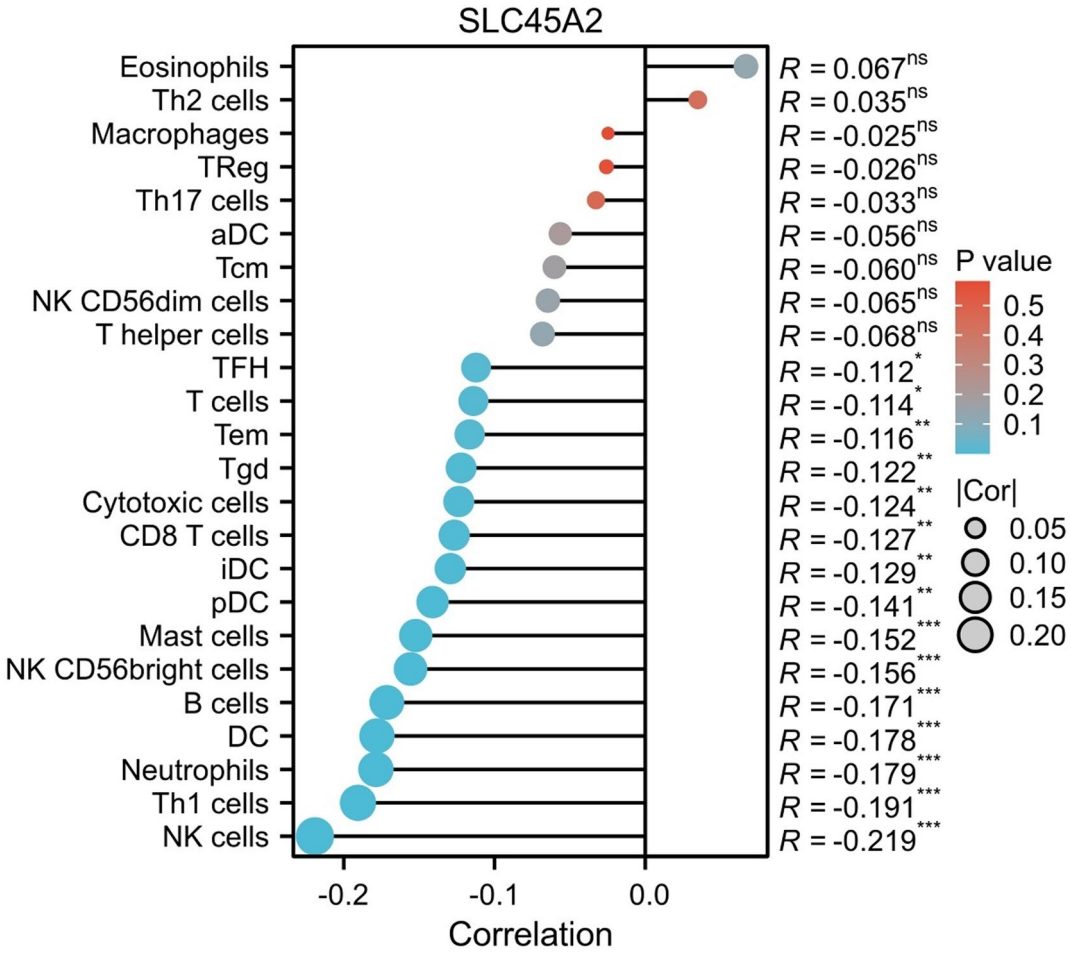

Fig. 3. Correlation analysis between SLC45A2 and immune cell infiltration in the PRAD tumor microenvironment. Spearman correlation analysis was performed to evaluate the association between SLC45A2 expression and immune infiltration, with results visualized using lollipop plots. The size of circles labeled "Cor" represents the magnitude of correlation coefficients, while *P* values indicate statistical significance. The left side of the bar plot lists immune cell types, and the right side displays R values reflecting the presence or absence of correlations.

Discussion

This study represents the first systematic elucidation of the oncogenic role and regulatory mechanisms of SLC45A2 in PRAD. Through multi-dimensional experimental approaches, we have demonstrated the following key findings: SLC45A2 exhibits significantly elevated expression in PRAD tumor tissues and serves as an independent prognostic factor. It promotes tumor proliferation and migration via activation of the PI3K/AKT signaling pathway, while mediating immune evasion by suppressing $CD8^+$T cell infiltration. The metabolic-immune axis formed through interactions with AMACR and ALB appears to represent a core regulatory mechanism. These discoveries not only fill a critical knowledge gap regarding SLC45A2's role in PRAD but also provide novel insights into the "metabolic-immune" crosstalk mechanisms underlying PRAD progression. The findings offer potential new avenues for therapeutic intervention targeting this metabolic-immune regulatory network.

Despite historical underinvestigation, SLC proteins are now recognized as critical players in fundamental biological processes and human diseases[26–29]. In cancer, dysregulation of SLC proteins has proven oncogenic[29–32]. For example, many SLCs are aberrantly expressed in lung adenocarcinoma (LUAD) and may serve as prognostic biomarkers[33,34]. Elevated SLC2A1 expression correlates with poor LUAD prognosis[35]. As for SLC45A2, inhibiting SLC45A2 was first shown to enhance melanosomal glycolysis and promote melanoma migration. Deleting SLC45A2 rendered melanoma cells more resistant to apoptosis and accelerated melanoma progression via PI3K/AKT pathway upregulation[36]. As a core pathway in tumor metabolic reprogramming, PI3K/AKT signaling modulates glycolysis by directly regulating glycolytic enzymes or controlling transcription factors[37]. Constitutively active AKT promotes HK2 activity and indirectly stimulates phosphofructokinase-1 activity[38]. AKT phosphorylates and increases pyruvate dehydrogenase kinase 1. PI3K/AKT signaling also mediates hypoxia-inducible factor 1, a key glycolytic transcription factor[39]. This study found that SLC45A2 knockdown downregulated AMACR, a key enzyme in PRAD fatty acid metabolism that supports tumor energy

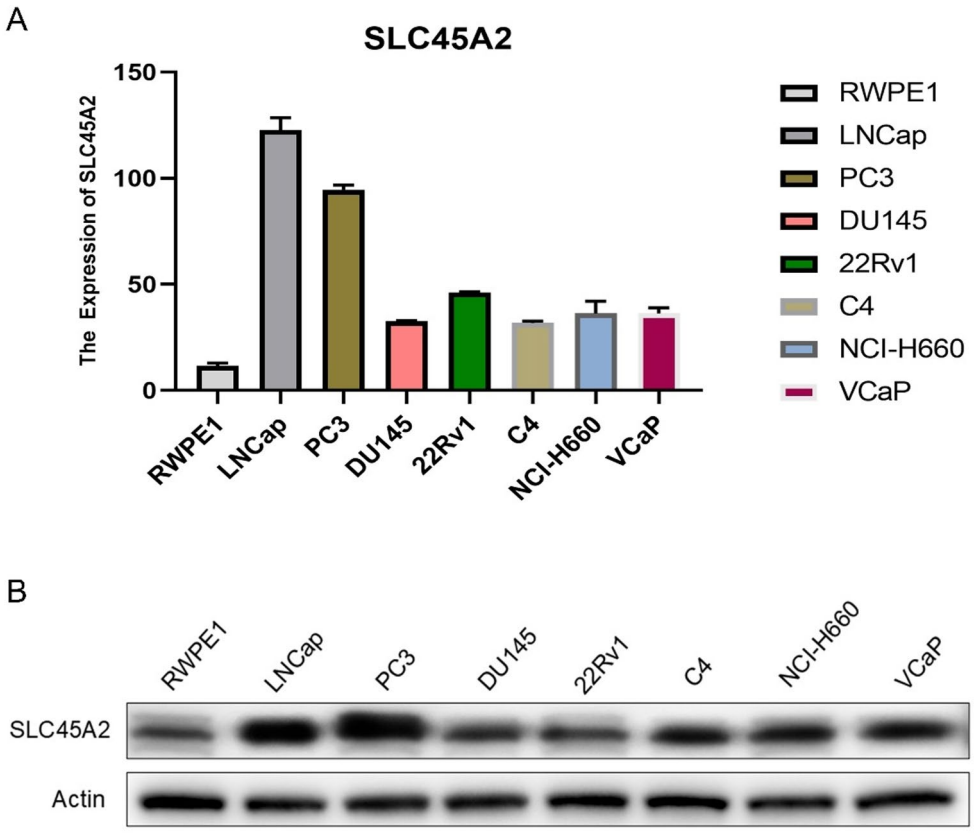

Fig. 4. Differential expression analysis of SLC45A2 in human prostate cells versus multiple cancer cell lines. (**A**) Analysis of SLC45A2 mRNA expression in human prostate cells and various cancer cell lines. (**B**) Analysis of SLC45A2 protein expression in human prostate cells and various cancer cell lines.

production via fatty acid β-oxidation, via PI3K/AKT pathway. This suggests that SLC45A2 may coordinate glycolysis and fatty acid metabolism through the "PI3K/AKT-AMACR" axis to provide metabolic substrates for tumor proliferation and migration. Additionally, the co-expression relationship between SLC45A2 and ALB supports this hypothesis, ALB may supply fatty acids for tumor energy, while SLC45A2 maintains metabolic microenvironment stability through ion transport regulation, synergistically promoting PRAD progression.

Through ssGSEA analysis, this study revealed a significant negative correlation between SLC45A2 overexpression and $CD8^+$T cell/NK cell infiltration, suggesting its potential role in mediating immune evasion by suppressing cytotoxic immune cell infiltration. Co-culture experiments with DU145 and $CD8^+$T cells confirmed that SLC45A2 knockdown enhanced $CD8^+$T cell-mediated tumor cell killing. This expands the role of SLC family genes in tumor immune regulation. Previous studies focused on SLC proteins inhibiting immune cell function via metabolic products[40,41], whereas this study is the first to demonstrate that SLC45A2 directly regulates immune cell infiltration to influence the PRAD immune microenvironment.

Potential mechanisms may involve SLC45A2-induced activation of the PI3K/AKT signaling pathway, which could promote the secretion of immunosuppressive factors that inhibit $CD8^+$ T-cell chemotaxis. In addition, SLC45A2–AMACR-mediated abnormalities in fatty acid metabolism may lower free fatty acid levels within the tumor microenvironment, thereby impairing the energy supply of $CD8^+$ T cells, which is consistent with previous reports showing that fatty acid deficiency drives $CD8^+$ T-cell exhaustion[41]. Moreover, SLC45A2 overexpression was positively correlated with the infiltration of MDSCs and Tregs, suggesting that it may facilitate immune evasion by enriching immunosuppressive cell populations. This hypothesis warrants further validation using flow cytometry-based immune cell profiling.

Limitations

Although this study elucidated the roles and mechanisms of SLC45A2 through a series of multi-dimensional experiments, several limitations remain. First, the limited number of normal tissue samples in the TCGA-PRAD dataset may reduce the robustness of the differential expression analysis. Second, only two prostate cancer cell lines were used for in vitro assays, and validation across additional models is lacking. Moreover, the precise mechanisms by which SLC45A2 regulates the PI3K/AKT signaling pathway and inhibits $CD8^+$ T-cell chemotaxis remain unclear. Further metabolomic profiling and ChIP assays are warranted to determine whether these interactions contribute to prostate cancer progression through metabolic or transcriptional modulation.

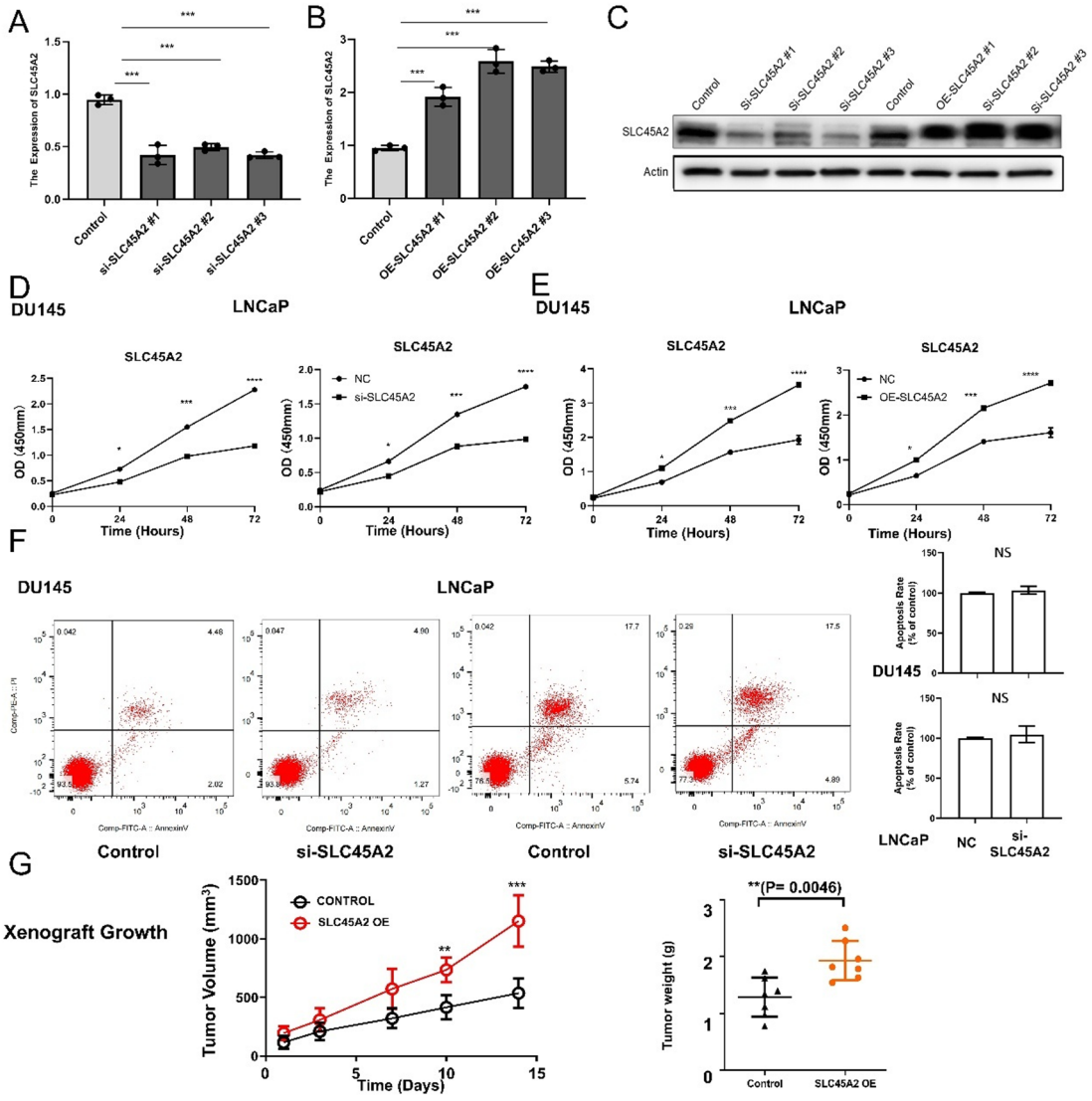

Fig. 5. SLC45A2 is closely associated with PRAD cell proliferation. (**A**–**B**) mRNA-level validation of SLC45A2 knockdown or overexpression in PRAD cells. (**C**) Protein-level validation of SLC45A2 knockdown or overexpression in PRAD cells. (**D**–**E**) CCK-8 assays demonstrate the effects of SLC45A2 knockdown and overexpression on PRAD cell proliferation in LNCaP and DU145 cells. (**F**) Effects of SLC45A2 on PRAD cell apoptosis detected by flow cytometry Cells were stained with Annexin V-FITC/PI and analyzed by flow cytometry. The quadrants represent different cell populations: lower left (viable cells), lower right (early apoptotic cells), upper right (late apoptotic or necrotic cells), and upper left (necrotic cells). (**G**) Xenograft analyses of DU145-derived tumors with control vector or SLC45A2 overexpression (**$P < 0.01$, ***$P < 0.001$).

Conclusion

In summary, this study demonstrates that SLC45A2 drives the progression of PRAD through a dual mechanism of "proliferation promotion and immune evasion." As an independent prognostic biomarker and a key molecule in the metabolic-immune axis, it offers a novel theoretical foundation and potential therapeutic targets for precision diagnosis and treatment of PRAD.

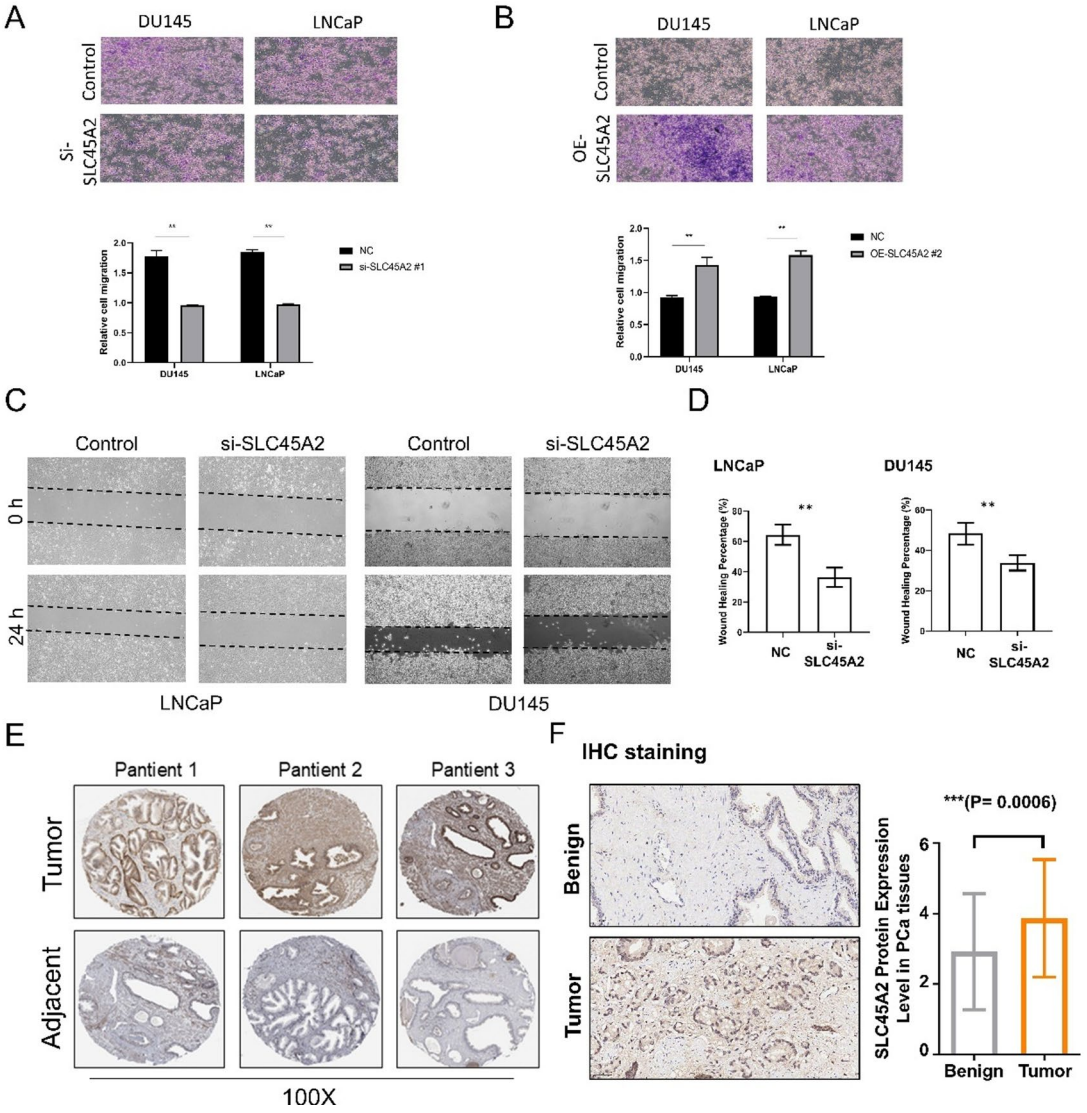

Fig. 6. SLC45A2 is closely associated with PRAD cell migration. (**A**) Transwell assays were conducted to assess the migration of DU145 and LNCaP cells after SLC45A2 knockdown (**$P < 0.01$). (**B**) Transwell assays were performed to evaluate the migration of DU145 and LNCaP cells following SLC45A2 overexpression (**$P < 0.01$). (**C**) Wound-healing assays validate the impact of SLC45A2 knockdown on PRAD cell migration in LNCaP and DU145 cells. (**D**) Quantification of wound-healing assay results. (**E**) IHC analysis of differential expression of SLC45A2 in PRAD tissue and adjacent tissues from HPA dataset. (**F**) Representative immunohistochemistry of PGM5 on PRAD tissue and adjacent tissues.

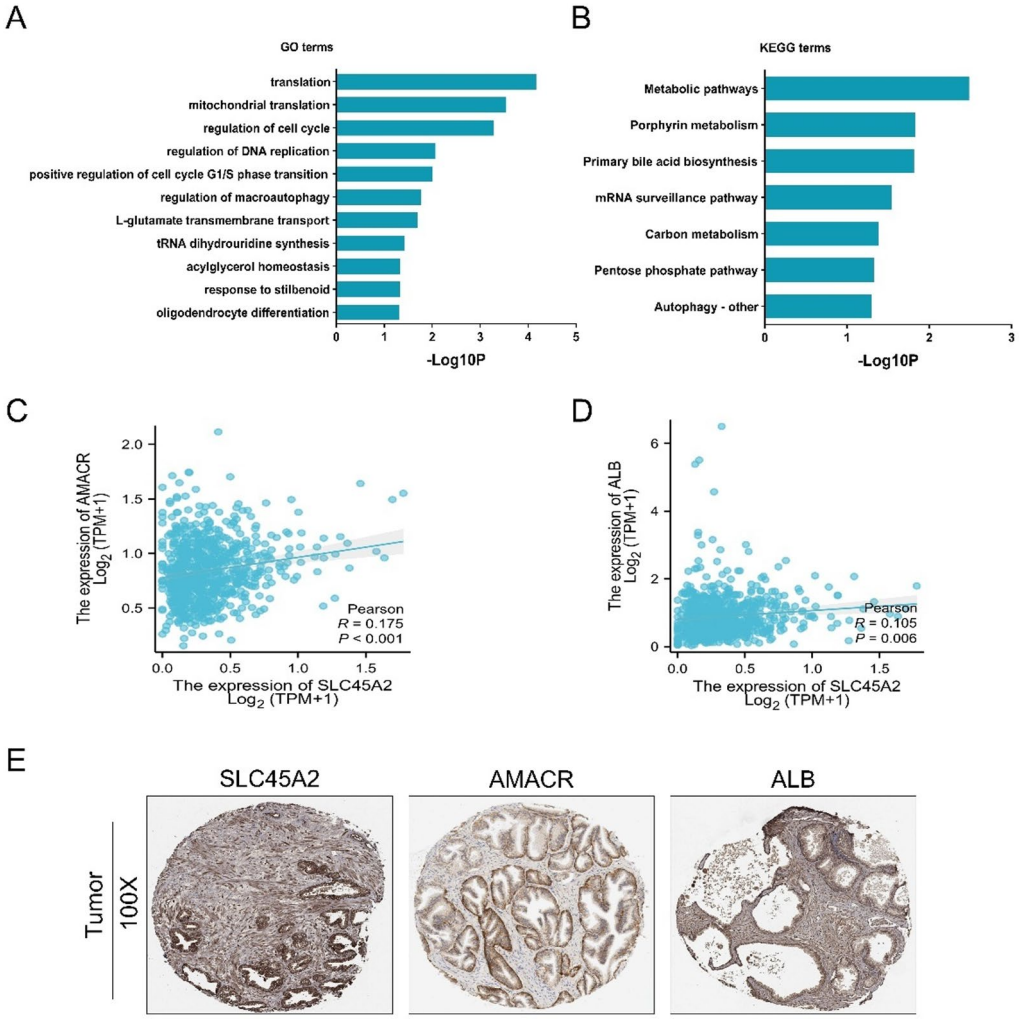

Fig. 7. IHC and correlation analysis of SLC45A2 with AMACR and ALB. (**A**) Bar plot of GO biological process enrichment. (**B**) Bar plot of KEGG pathway enrichment [21–25]. Copyright permission of KEGG pathway maps our manuscript has been obtained. (**C**–**D**) mRNA expression correlation analysis of SLC45A2 with AMACR and ALB based on TCGA transcriptomic data. (**E**) Protein expression correlation analysis of SLC45A2 with AMACR and ALB based on HPA immunohistochemistry data.

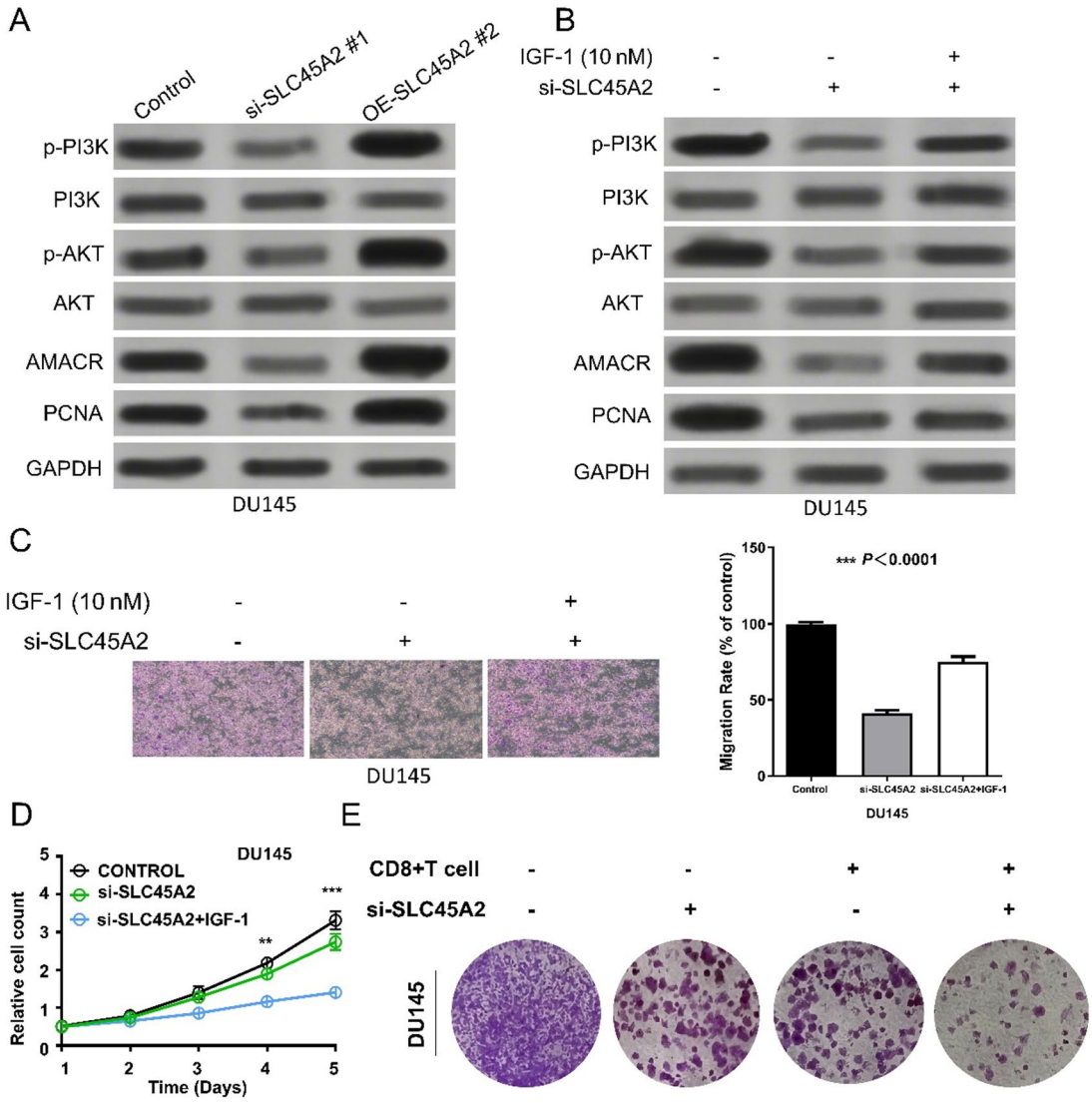

Fig. 8. Analysis of signaling pathways and immune cell co-culture assays. (**A**) Western blot analysis of p-PI3K, PI3K, p-AKT, AKT, AMACR, PCNA, and GAPDH protein levels in DU145 cells. (**B**) Western blot analysis of p-PI3K, PI3K, p-AKT, AKT, AMACR, PCNA, and GAPDH in control and SLC45A2-knockdown DU145 cells treated with IGF-1. (**C**) Transwell migration assay assessing the migratory ability of control and SLC45A2-knockdown DU145 cells following IGF-1 treatment (**$P<0.01$). (**D**) CCK-8 assay evaluating the proliferative capacity of control and SLC45A2-knockdown DU145 cells treated with IGF-1. (**E**) Effects of SLC45A2 knockdown combined with $CD8^+$ T-cell co-culture on DU145 cell proliferation. Viable cells were visualized by crystal violet staining; purple-stained cells represent surviving DU145 cells. Differences in staining intensity and distribution reflect cell viability under various treatment conditions. "–" indicates absence of treatment; "+" indicates presence of treatment.

Data availability

The datasets used and/or analyzed during the current study available from the corresponding author on reasonable request.

Received: 9 June 2025; Accepted: 9 December 2025
Published online: 15 December 2025

References

1. Naranjo, N. M. et al. Neuroendocrine gene subsets are uniquely dysregulated in prostate adenocarcinoma. *Cancer Biol. Ther.* **25**, 2364433. https://doi.org/10.1080/15384047.2024.2364433 (2024).
2. Zaidi, S. et al. Single-cell analysis of treatment-resistant prostate cancer: implications of cell state changes for cell surface antigen-targeted therapies. *Proc. Natl. Acad. Sci. U S A.* **121**, e2322203121. https://doi.org/10.1073/pnas.2322203121 (2024).
3. Yu, T. et al. Targeting tumor-intrinsic SLC16A3 to enhance anti-PD-1 efficacy via tumor immune microenvironment reprogramming. *Cancer Lett.* **589**, 216824. https://doi.org/10.1016/j.canlet.2024.216824 (2024).

4. Li, Y. et al. Epigenetic-related gene-based prognostic model construction and validation in prostate adenocarcinoma. *Heliyon* **10**, e30941. https://doi.org/10.1016/j.heliyon.2024.e30941 (2024).
5. Liu, S., Yu, Y., Xu, J., Wang, Y. & Li, D. Single-cell and bulk RNA-sequencing reveals mitosis-involved gene HAUS1 is a promising indicator for predicting prognosis and immune responses in prostate adenocarcinoma (PRAD). *Cell. Biol. Int.* **48**, 1169–1184. https://doi.org/10.1002/cbin.12191 (2024).
6. Le, J., Chen, Y., Yang, W., Chen, L. & Ye, J. Metabolic basis of solute carrier transporters in treatment of type 2 diabetes mellitus. *Acta Pharm. Sin B.* **14**, 437–454. https://doi.org/10.1016/j.apsb.2023.09.004 (2024).
7. Schlessinger, A., Zatorski, N., Hutchinson, K. & Colas, C. Targeting SLC transporters: small molecules as modulators and therapeutic opportunities. *Trends Biochem. Sci.* **48**, 801–814 (2023).
8. Pizzagalli, M. D., Bensimon, A. & Superti-Furga, G. A guide to plasma membrane solute carrier proteins. *FEBS J.* **288**, 2784–2835 (2021).
9. Pizzagalli, M. D., Bensimon, A. & Superti-Furga, G. A guide to plasma membrane solute carrier proteins. *FEBS J.* **288**, 2784–2835. https://doi.org/10.1111/febs.15531 (2021).
10. Schumann, T. et al. Solute carrier transporters as potential targets for the treatment of metabolic disease. *Pharmacol. Rev.* **72**, 343–379. https://doi.org/10.1124/pr.118.015735 (2020).
11. Weiss, J. M. et al. Regulatory T cells and myeloid-derived suppressor cells in the tumor microenvironment undergo Fas-dependent cell death during IL-2/αCD40 therapy. *J. Immunol.* **192**, 5821–5829. https://doi.org/10.4049/jimmunol.1400404 (2014).
12. Yang, B. et al. TRIM35 triggers cardiac remodeling by regulating SLC7A5-mediated amino acid transport and mTORC1 activation in fibroblasts. *Cell. Commun. Signal.* **22**, 444. https://doi.org/10.1186/s12964-024-01826-0 (2024).
13. Dvorak, V. et al. Paralog-dependent isogenic cell assay cascade generates highly selective SLC16A3 inhibitors. *Cell. Chem. Biol.* **30** https://doi.org/10.1016/j.chembiol.2023.06.029 (2023).
14. Klouwer, F. C. et al. Redefining the phenotype of alpha-methylacyl-CoA racemase (AMACR) deficiency. *Orphanet J. Rare Dis.* **19**, 350 (2024).
15. Yang, L., Shao, Y., Gao, T., Bajinka, O. & Yuan, X. Current advances in cancer energy metabolism under dietary restriction: a mini review. *Med. Oncol.* **41**, 209 (2024).
16. Nóbrega, M. et al. Association of polymorphisms of PTEN, AKT1, PI3K, AR, and AMACR genes in patients with prostate cancer. *Genet. Mol. Biology*. **43**, e20180329 (2020).
17. Yan, C., Niu, Y., Li, F., Zhao, W. & Ma, L. System analysis based on the pyroptosis-related genes identifies GSDMC as a novel therapy target for pancreatic adenocarcinoma. *J. Transl Med.* **20**, 455. https://doi.org/10.1186/s12967-022-03632-z (2022).
18. Ma, Z. et al. Identification and analysis of mitochondria-related central genes in steroid-induced osteonecrosis of the femoral head, along with drug prediction. *Front. Endocrinol. (Lausanne).* **15**, 1341366. https://doi.org/10.3389/fendo.2024.1341366 (2024).
19. Khlebus, E. et al. Comparative tumor microenvironment analysis of primary and recurrent ovarian granulosa cell tumors. *Mol. Cancer Res.* **21**, 483–494. https://doi.org/10.1158/1541-7786.MCR-22-0623 (2023).
20. Dai, D. L., Martinka, M. & Li, G. Prognostic significance of activated Akt expression in melanoma: a clinicopathologic study of 292 cases. *J. Clin. Oncol.* **23**, 1473–1482. https://doi.org/10.1200/JCO.2005.07.168 (2005).
21. Dennis, G. Jr. et al. Database for annotation, visualization, and integrated discovery. *Genome Biol.* **4**, P3 (2003).
22. Kanehisa, M. & Goto, S. KEGG: Kyoto encyclopedia of genes and genomes. *Nucleic Acids Res.* **28**, 27–30. https://doi.org/10.1093/nar/28.1.27 (2000).
23. Kanehisa, M. Toward Understanding the origin and evolution of cellular organisms. *Protein Sci.* **28**, 1947–1951. https://doi.org/10.1002/pro.3715 (2019).
24. Kanehisa, M., Furumichi, M., Sato, Y., Kawashima, M. & Ishiguro-Watanabe, M. KEGG for taxonomy-based analysis of pathways and genomes. *Nucleic Acids Res.* **51**, D587–d592. https://doi.org/10.1093/nar/gkac963 (2023).
25. Kanehisa, M., Furumichi, M., Sato, Y., Matsuura, Y. & Ishiguro-Watanabe, M. KEGG: biological systems database as a model of the real world. *Nucleic Acids Res.* **53**, D672–D677 (2025).
26. César-Razquin, A. et al. A call for systematic research on solute carriers. *Cell* **162**, 478–487. https://doi.org/10.1016/j.cell.2015.07.022 (2015).
27. Rotow, J. & Bivona, T. G. Understanding and targeting resistance mechanisms in NSCLC. *Nat. Rev. Cancer*. **17**, 637–658. https://doi.org/10.1038/nrc.2017.84 (2017).
28. Schaller, L. & Lauschke, V. M. The genetic landscape of the human solute carrier (SLC) transporter superfamily. *Hum. Genet.* **138**, 1359–1377. https://doi.org/10.1007/s00439-019-02081-x (2019).
29. Xie, L. et al. Solute carrier protein family May involve in radiation-induced radioresistance of non-small cell lung cancer. *J. Cancer Res. Clin. Oncol.* **137**, 1739–1747. https://doi.org/10.1007/s00432-011-1050-9 (2011).
30. Mohelnikova-Duchonova, B. et al. The association between the expression of solute carrier transporters and the prognosis of pancreatic cancer. *Cancer Chemother. Pharmacol.* **72**, 669–682. https://doi.org/10.1007/s00280-013-2246-2 (2013).
31. Bhutia, Y. D. et al. SLC transporters as a novel class of tumour suppressors: Identity, function and molecular mechanisms. *Biochem. J.* **473**, 1113–1124. https://doi.org/10.1042/BJ20150751 (2016).
32. Sutherland, R., Meeson, A. & Lowes, S. Solute transporters and malignancy: Establishing the role of uptake transporters in breast cancer and breast cancer metastasis. *Cancer Metastasis Rev.* **39**, 919–932. https://doi.org/10.1007/s10555-020-09879-6 (2020).
33. Ikeda, K. et al. Prognostic significance of aberrant methylation of solute carrier gene family 5A8 in lung adenocarcinoma. *Ann. Thorac. Surg.* **99**, 1755–1759. https://doi.org/10.1016/j.athoracsur.2015.02.013 (2015).
34. Lehrer, S. & Rheinstein, P. H. Expression of the vesicular monoamine transporter gene solute carrier family 18 member 1 (SLC18A1) in lung cancer. *Cancer Genomics Proteom.* **15**, 387–393. https://doi.org/10.21873/cgp.20097 (2018).
35. Guo, W. et al. Elevated SLC2A1 expression correlates with poor prognosis in patients with surgically resected lung adenocarcinoma: A study based on immunohistochemical analysis and bioinformatics. *DNA Cell. Biol.* **39**, 631–644. https://doi.org/10.1089/dna.2019.5291 (2020).
36. Liu, Y. et al. Ablation of Proton/Glucose exporter SLC45A2 enhances melanosomal Glycolysis to inhibit melanin biosynthesis and promote melanoma metastasis. *J. Invest. Dermatol.* **142** https://doi.org/10.1016/j.jid.2022.04.008 (2022).
37. Hoxhaj, G. & Manning, B. D. The PI3K-AKT network at the interface of oncogenic signalling and cancer metabolism. *Nat. Rev. Cancer*. **20**, 74–88. https://doi.org/10.1038/s41568-019-0216-7 (2020).
38. Journiac, N. et al. Cell metabolic alterations due to Mcph1 mutation in microcephaly. *Cell. Rep.* **31**, 107506. https://doi.org/10.1016/j.celrep.2020.03.070 (2020).
39. Fojtík, P., Beckerová, D., Holomková, K., Šenfluk, M. & Rotrekl, V. Both hypoxia-inducible factor 1 and MAPK signaling pathway attenuate PI3K/AKT via suppression of reactive oxygen species in human pluripotent stem cells. *Front. Cell. Dev. Biol.* **8**, 607444. https://doi.org/10.3389/fcell.2020.607444 (2020).
40. Li, C. et al. SLC16A3 is a prognostic marker and affects immune regulation in bladder cancer. *Comb. Chem. High. Throughput Screen.* https://doi.org/10.2174/0113862073278304240614064748 (2024).
41. Yan, C. et al. Upregulation of SLC12A3 and SLC12A9 mediated by the HCP5/miR-140-5p axis confers aggressiveness and unfavorable prognosis in uveal melanoma. *Lab. Invest.* **103**, 100022. https://doi.org/10.1016/j.labinv.2022.100022 (2023).

Acknowledgements
KEGG pathway database is copyrighted by Kanehisa laboratories and we have formal permission from them to publish this material commercially under an Open Access license.

Author contributions
R.T. and Z.M.W.: conception and design, obtaining funding and drafting the manuscript; R.T. and C.W.: acquisition of the data and drafting the manuscript; R.T.: IHC assay; R.T. and Y.X.Z.: in vitro and in vivo assays; R.T. and Z.M.W.: critical revision of the manuscript; Y.X.Z. and K.L.: statistical analysis and technical support.

Declarations

Competing interests
The authors declare no competing interests.

Ethical approval and consent to participate
The protocol of experiments involving human participants has been approved by the medical ethical committee of The People's Hospital of Suzhou New District and has followed the principles outlined in the Declaration of Helsinki for all human or animal experimental investigations. Our study was reported as described by the ARRIVE guidelines. Informed consent was obtained from all subjects.

Additional information
Supplementary Information The online version contains supplementary material available at https://doi.org/10.1038/s41598-025-32340-z.

Correspondence and requests for materials should be addressed to Z.W.

Reprints and permissions information is available at www.nature.com/reprints.

Publisher's note Springer Nature remains neutral with regard to jurisdictional claims in published maps and institutional affiliations.

Open Access This article is licensed under a Creative Commons Attribution-NonCommercial-NoDerivatives 4.0 International License, which permits any non-commercial use, sharing, distribution and reproduction in any medium or format, as long as you give appropriate credit to the original author(s) and the source, provide a link to the Creative Commons licence, and indicate if you modified the licensed material. You do not have permission under this licence to share adapted material derived from this article or parts of it. The images or other third party material in this article are included in the article's Creative Commons licence, unless indicated otherwise in a credit line to the material. If material is not included in the article's Creative Commons licence and your intended use is not permitted by statutory regulation or exceeds the permitted use, you will need to obtain permission directly from the copyright holder. To view a copy of this licence, visit http://creativecommons.org/licenses/by-nc-nd/4.0/.

© The Author(s) 2025